Maneuver at Micro Scale: Steering by Actuation Frequency Control in Micro Bristle Robots*

Zhijian Hao[1], DeaGyu Kim[1], Ali Reza Mohazab[2] and Azadeh Ansari[1]

Abstract— This paper presents a novel steering mechanism, which leads to frequency-controlled locomotion demonstrated for the first time in micro bristle robots. The miniaturized robots are 3D-printed, 12 mm × 8 mm × 6 mm in size, with bristle feature sizes down to 400 μm. The robots can be steered by utilizing the distinct resonance behaviors of the asymmetrical bristle sets. The left and right sets of the bristles have different diameters, and thus different stiffnesses and resonant frequencies. The unique response of each bristle side to the vertical vibrations of a single on-board piezoelectric actuator causes differential steering of the robot. The robot can be modeled as two coupled uniform bristle robots, representing the left and the right sides. At distinct frequencies, the robots can move in all four principal directions: forward, backward, left and right. Furthermore, the full 360° 2D plane can be covered by superimposing the principal actuation frequency components with desired amplitudes. In addition to miniaturized robots, the presented resonance-based steering mechanism can be applied over multiple scales and to other mechanical systems.

Fig. 1. a) An asymmetrical bristle design of the steerable micro bristle robot. Each side has 8 bristles with diameters of 800/400 μm. b) The 3D-printed bristle robot body in comparison with a US penny.

I. INTRODUCTION AND RELATED WORK

In this paper, we present a reliable mechanism to enable frequency-controlled steering of micro bristle robots in all directions for the first time. We take advantage of an asymmetrical bristle design, along with the structural resonance behavior of the bristles (Fig. 1). The presented steering mechanism only requires a single actuator (e.g. piezoelectric actuator) on a unibody robot, and is thus preferred in smaller-scale applications.

Bristle robots use bristles' stick-slip cycle under vibration, which generates asymmetrical frictional forces, to achieve locomotion [1-21]. Previous works on bristle robots have mainly focused on the macro scales where the robots are larger than 1 cm in each dimension [1-8]. These macro-scale robots can be classified into non-steerable or steerable robots.

Non-steerable vibration-driven bristle robots are demonstrated to be suitable for applications within confined spaces (such as in pipe inspections [3,6,8,14]), as well as earthquake rescue [15]. In addition to vibration-driven bristle robots, soft bristle robots can achieve stick-slip locomotion through the assist of soft and deformable sections [16,17]. In such sys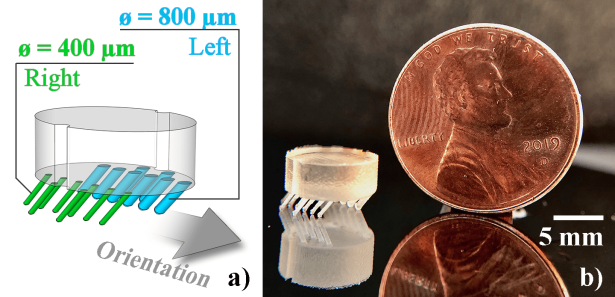tems, the contraction/relaxation cycle of the main body, coupled with the interlock/release cycle of the bristles, produces the unidirectional locomotion. Amongst these examples, either strict motion constraints are applied (as in pipe-following bristle robots) or only unidirectional motion is achieved (as in soft bristle robots). While these robots only use a single actuator, which is favorable for down scaling, the lack of steerability limits their applications in unconstrained environments.

To achieve steering, macro-scale bristle robots utilize multiple actuators, as reported in [1,4,18,19,26]. The dynamics of such systems are modeled in [18], where two vibration sources can be individually controlled to actuate each side of the robot, in order to achieve differential steering. However, such scheme is less desirable for miniaturization, as integrating more components poses additional manufacturing challenges. In addition, unwanted mechanical coupling due to the proximity of multiple actuators at micro scales renders such differential steering mechanisms impractical. Therefore, to build controllable bristle robots at micro scales, a simple and robust steering mechanism that does not require complex actuator integration is needed.

As shown in Fig. 2, the authors have demonstrated micro bristle robots with a uniform bristle design and a bristle diameter of 100 μm, fabricated by two-photon polymerization [20]. The robot can achieve a speed up to 4 times its body length per second, when actuated on a piezoelectric shaker. As predicted by the theory, the robots are capable of bidirectional motion (forward and backward) when actuated at different frequencies [21]. However, full steering (360° in the 2D plane), has not been achieved for micro bristle robots to date, and is the focus of this work.

[1]Zhijian Hao, DeaGyu Kim, and Azadeh Ansari are with the School of Electrical and Computer Engineering at the Georgia Institute of Technology, Atlanta, GA 30308 USA. `zhao38@gatech.edu`, `dkim439@gatech.edu`, `azadeh.ansari@ece.gatech.edu`

[2]Ali Reza Mohazab is with the Foundation for the Advancement of Sciences, Humanities, Engineering, and Arts, FASHEA, Richmond, BC, Canada. `ali.mohazab@fashea.org`
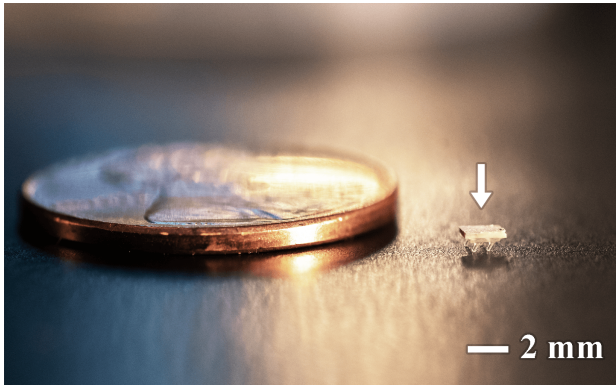
Fig. 2. A micro bristle robot fabricated with two-photon polymerization in comparison with a US penny. The bristle diameter is 100 μm. The robot could achieve bidirectional (forward and backward) locomotion at distinct frequencies.

II. PROBLEM STATEMENT AND METHOD OVERVIEW

Many traditional macro-scale robotic actuation and steering mechanisms require complex components and are not desirable in micro robots due to manufacturing considerations, unwanted mechanical couplings, and the scaling law of actuation forces [22]. A simple and robust actuation mechanism that can generate large enough thrust to overcome the adhesive forces at micro scales with steering capability is the focus of this work.

We designed an asymmetrical bristle robot with bristles on the left and right sides of the robot having different diameters and thus different stiffnesses and resonant frequencies. At these resonance frequencies, the amplitude of the vibration will be amplified by the quality factor, Q, of the structure, which can help generate larger forces. By altering vibration frequencies, the bristles sets generate asymmetrical forces that can differentially drive the robot and change its direction.
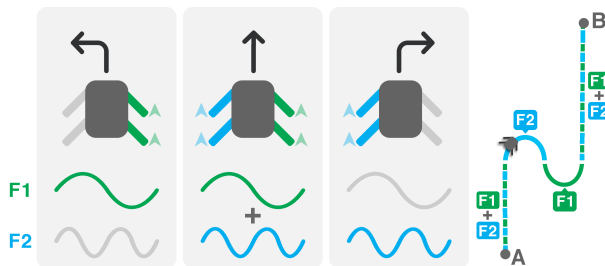

Fig. 3. Steering is achieved when actuated at frequencies corresponding to the resonance of each bristle set. A superposition of two frequencies can be used to achieve more directions of motion.

When the on-board piezoelectric actuator operates at a certain frequency, the left/right side move faster than the other side, causing a right/left turn (Fig. 3). It is also expected to move in minor directions that form an angle with the mentioned four principal directions when two frequencies are superimposed.

This mechanism is especially preferred for miniaturized robots in micro/millimeter scales. The fact that steering can

be achieved in a unibody design, with no moving components and with only a single actuator, simplifies the complex fabrication processes, associated with the micro-robots.

Micro bristle robots with an overall size of 12 mm $\times$ 8 mm $\times$ 6 mm and bristle diameters down to 400 and 800 μm were fabricated by 3D printing and the experimental results will be shown in the following sections.
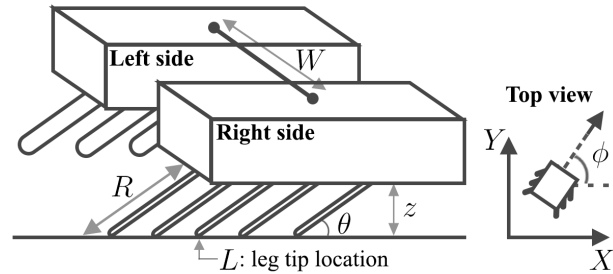
III. STEERING MECHANISM MODELING

Fig. 4. The asymmetrical robot is modeled as two coupled bristle robots each with uniform bristles, with a separation distance W.

The steerable robot with asymmetrical bristle design can be modeled as two coupled bristle robots each having a set of uniform bristles (Fig. 4). By changing the bristle dimensions on each side, we can design different torsional spring constants (κ) and thus different resonant frequencies at the stiction regime (ω_θ) and slipping regime (ω). The expression for the resonant frequencies at these regimes for each side (adapted from [21]) can be written as:

$$\omega^2 = \frac{\omega_\theta^2 / \cos^2 \bar{\theta}}{1 + \frac{\dot{\vec{L}} \cdot \hat{n}}{\dot{\vec{L}} \cdot \dot{\vec{L}}} \mu_k \tan \bar{\theta}} \tag{1a}$$

, where

$$\omega_\theta^2 = \left(\frac{\kappa}{mR^2} \right) \left(1 + (\bar{\theta} - \theta_0) \tan \bar{\theta} \right) \tag{1b}$$

In the above equation, θ_0 is the fabricated angle of bristles under no load, $\bar{\theta}$ is the equilibrium bristle angle when the system is under gravity, μ_k is the coefficient of kinetic friction, and $\vec{L}$ denotes the location of bristle tips. Note that the kinetic friction term only applies when the bristle tips are in motion (i.e. $\dot{\vec{L}} \neq 0$).

We assume that all bristles move in unison back and forth along the orientation axis. We further identify 3 degrees of freedom: X, Y, ϕ, where, X, Y denote the center of mass position, and ϕ denotes the orientation. For a given actuation frequency at a certain amplitude, the forces exerted by the two sides of the compound robot are different in magnitude and sometimes different in direction, causing the robot to steer. Assuming small amplitudes and a single mode of vibration, the independent equations of motion for each simple robot can be written as follows:

During the slip phase ($\dot{\vec{L}} \neq 0$):

$$\begin{cases} \ddot{z} = -\omega^2(z - \bar{z}) - \ddot{\eta}(t) \\ \ddot{q} = -\mu_k[\ddot{z} + g + \ddot{\eta}(t)]\frac{\dot{\vec{L}} \cdot \hat{n}}{\dot{\vec{L}} \cdot \dot{\vec{L}}} \end{cases} \quad (2a)$$

During the stick phase ($\dot{\vec{L}} = 0$):

$$\begin{cases} \dot{z} = R\dot{\theta}\cos\theta \\ \dot{q} = -R\dot{\theta}\sin\theta \\ \ddot{\theta} = -\left(\omega_\theta^2 - \frac{\ddot{\eta}(t)\sin\bar{\theta}}{R}\right)(\theta - \bar{\theta}) - \left(\frac{\cos\bar{\theta}}{R}\right)\ddot{\eta}(t) \end{cases} \quad (2b)$$

, where z is the vertical displacement of the body, $\bar{z}$ is the equilibrium height when the bristles are slipping on the ground (note that the equilibrium height will be different depending on whether the bristles slip forward or backward [21]), g is the acceleration of gravity, $\hat{n}$ is the 2D orientation vector of the full robot: $\cos\phi\hat{i} + \sin\phi\hat{j}$, $\ddot{\eta}(t)$ is the force function of the on-board vibration source divided by the mass of the robot, q is the horizontal displacement of bristle tips along the orientation, and R is the bristle length.

The transition from the stick to the slip cycle happens when:

$$\begin{aligned} |R\ddot{\theta}\sin\theta + \dot{\theta}^2 R\cos\theta| \\ > \mu_s|R\ddot{\theta}\cos\theta - R\dot{\theta}^2\sin\theta + g + \ddot{\eta}(t)| \end{aligned} \quad (3a)$$

, where μ_s is the static coefficient of friction. The transition back happens when the condition is reversed. Note that the system can be driven by a ground shaker as shown in [19], wherein $\eta(t)$ is the kinematic function of the ground shaker.

The above equations apply to both sides of the robot with different ω_θ values. The ideal orientation and trajectory of the asymmetrical bristle robot along with the motion of bristle tips can be described as:

$$\begin{cases} \ddot{\phi} = \frac{\ddot{q}_{(R)} - \ddot{q}_{(L)}}{W/2} \\ \ddot{X} = \frac{\ddot{q}_{(R)} + \ddot{q}_{(L)}}{2}\cos\phi \\ \quad - \mu_k \sum_{i=L,R}\left[\frac{([\dot{\vec{L}}_{(i)} - (\dot{\vec{L}}_{(i)} \cdot \hat{n})\hat{n}] \cdot \hat{i})[\ddot{z}_{(i)} + g + \ddot{\eta}(t)]}{2|\dot{\vec{L}}_{(i)}|}\right] \\ \ddot{Y} = \frac{\ddot{q}_{(R)} + \ddot{q}_{(L)}}{2}\sin\phi \\ \quad - \mu_k \sum_{i=L,R}\left[\frac{([\dot{\vec{L}}_{(i)} - (\dot{\vec{L}}_{(i)} \cdot \hat{n})\hat{n}] \cdot \hat{j})[\ddot{z}_{(i)} + g + \ddot{\eta}(t)]}{2|\dot{\vec{L}}_{(i)}|}\right] \end{cases}$$
$$(4)$$

$$\begin{cases} \dot{\vec{L}}_{(L)} = \frac{z_{(L)}\dot{z}_{(L)}}{\sqrt{R_{(L)}^2 - z_{(L)}^2}}\hat{n} - \frac{W\dot{\phi}}{2}\hat{n} + \dot{X}\hat{i} + \dot{Y}\hat{j} \\ \dot{\vec{L}}_{(R)} = \frac{z_{(R)}\dot{z}_{(R)}}{\sqrt{R_{(R)}^2 - z_{(R)}^2}}\hat{n} + \frac{W\dot{\phi}}{2}\hat{n} + \dot{X}\hat{i} + \dot{Y}\hat{j} \end{cases} \quad (5)$$

, where subscripts $_{(L)}$ and $_{(R)}$ denote the side of the robot, $\ddot{q}$ and $\dot{z}$ are obtained from (2), W is the separation between the two sides, and the $\sum$ terms account for the lateral direction sliding.

The system equations predict different frequency responses of the left/right sides' speeds. Numerically solving

the equations for q to get the steady state average speed for different frequencies, we obtain the following representative plots (Fig. 5a). The different directions of motion can thus be predicted by the average and differential speeds of left/right bristles (Fig. 5b).
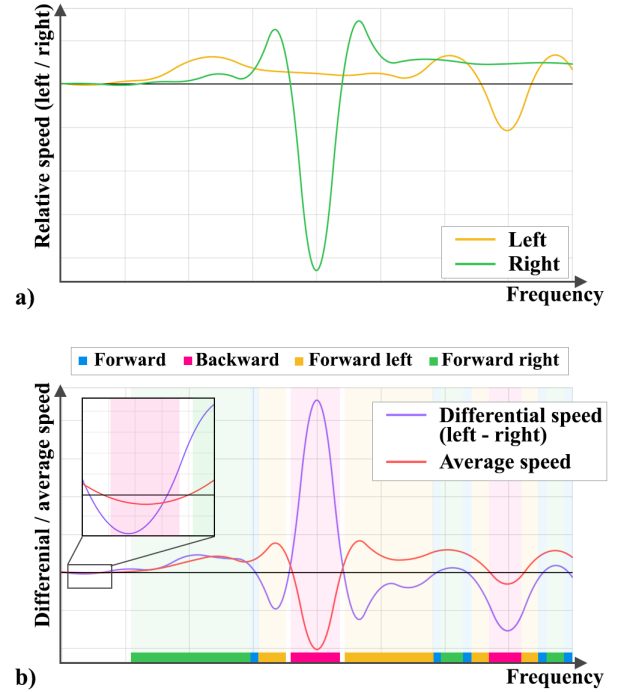

Fig. 5. Numerical simulation results based on the model: a) Left and right bristles' speed vs. frequency, and b) average and differential speed between the two sides, with color coded predicted direction of motion. In this sample calculation, the bristle angle is $45°$, $\mu_s = 0.4$, and $\mu_k = 0.3$.

If one is interested in the steady state behavior and the macroscopic trajectory of the robot, one can integrate (4), to get $\dot{\phi} = \frac{\dot{q}_{(R)} - \dot{q}_{(L)}}{W/2}$, assuming initial rotational speed of zero. We know that in the steady state $\bar{q}$ is constant, which corresponds to the steady state speed of the uniform bristle robot. Therefore, $\dot{\phi}$ is proportional to the difference of the speed of the two sides and is a constant in the steady state. Furthermore assuming that the robot does not slide sideways in the steady state, the rigidity of the robot body dictates that the robot travels on circular arcs obeying:

$$\frac{\bar{\dot{q}}_{(L)}}{\bar{\dot{q}}_{(R)}} = \frac{\rho_{(L)}}{\rho_{(R)}} = \frac{\rho_{(L)}}{W + \rho_{(L)}} \quad (6)$$

Hence the arc trajectory for the center of mass is a circle with $\rho = \rho_{(L)} + W/2$, where $\rho < 0$ indicates arching down and $\rho > 0$ indicates arching up. Solving for ρ, one gets:

$$\rho = \frac{W\bar{\dot{q}}_{(L)}}{\bar{\dot{q}}_{(R)} - \bar{\dot{q}}_{(L)}} + \frac{W}{2} \quad (7)$$

It is worth mentioning that, in terms of the quantitative behavior (such as frequency and speed values), the actual robot system is far more complicated than the simplified ideal model developed above, considering 1) the couplings within each set of bristles allowing for more complex modes,

2) the fabrication errors and material nonidealities, 3) the actuator non-linearities, as well as 4) the loading effect of the tethering wires in the current setup. However, the model provides insights and design guidance on the presented steerable robot.

IV. FABRICATION AND TEST SETUP

The presented robot consists of three main components: a polymer body with two asymmetrical bristle sets (on the left and right sides), a PZT (lead zirconate titanate) plate as the vibration source, and wires that deliver power to the PZT actuator. The on-board PZT actuator and wires can be replaced with external vibration sources, such as a piezoelectric shaker, set beneath the robot. This would eliminate the use of wires. However, this work is an intermediate step towards the realization of an autonomous and untethered system, where an on-board battery will be used to power the actuator, and thus eliminate the use of wires. The assembled micro bristle robot is shown in Fig. 6.
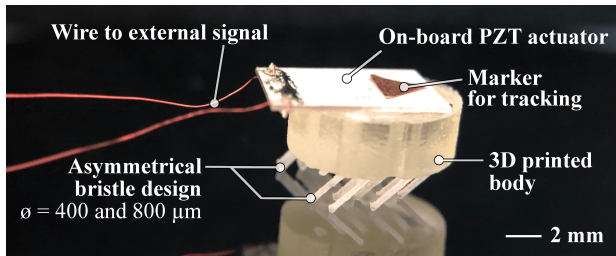

Fig. 6. An assembled micro bristle robot (12 mm × 8 mm × 6 mm) consisting of an on-board PZT actuator and a 3D-printed body.

The polymer body and bristles were 3D printed using Project 3510 HD made by 3DSYSTEMS [23]. The material used was VisiJet M3 Crystal. The material's mechanical properties can be found in [24]. The body is an elliptic cylinder (h = 3.4 mm, a = 5 mm, b = 4 mm), which prevents the robot from getting stuck to obstacles and during collisions. Two sets of 8 bristles were printed under the body, with diameters of 800/400 μm for the left/right side. The bristle length is 3 mm, and the tilt angle is 45°.

The PZT plate was purchased from APC International (made of material 851) and was diced into 10 mm × 6 mm × 0.3 mm pieces. The material properties can be found in [25]. The diced PZT piece was soldered with Copper Magnet Wire (MW0099, TEMCo) and attached to the top of the 3D-printed body.

The test setup is shown in Fig. 7. Sinusoidal signals at various frequencies were generated by a two-channel function generator (33500B, Agilent). Depending on whether the superposition of two frequencies was needed, the signals were either first mixed using an adding circuit built with an op-amp (UA741, Texas Instruments) or directly fed into the voltage amplifier (7602M, Krohn-Hite). The DC supply (E3620A, Keysight) was used to supply the DC voltage to the op-amp. The pre-amplification signal was monitored using an oscilloscope (DSOX4024A, Keysight) showing the voltage for each frequency component. The amplified signals were

input via wires to actuate the on-board PZT. The robot was placed on a tempered glass surface, and the motion of the robot was recorded by a camera.
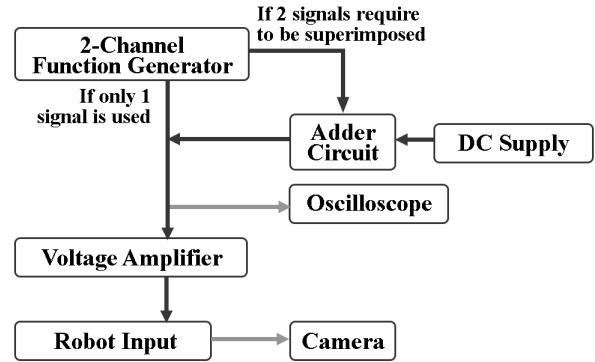

Fig. 7. Test setup.

V. EXPERIMENTAL RESULTS

A. Steering at Different Actuation Frequencies

The robot was placed to face right (0°) with the wires extended to the left (180°). The tested frequency range was 1-120 kHz. When a pure sinusoidal signal with a single frequency component and an amplitude of 40 V was applied to the PZT actuator, the micro bristle robot showed frequency dependent locomotion in all four principal directions: forward, backward, left and right.
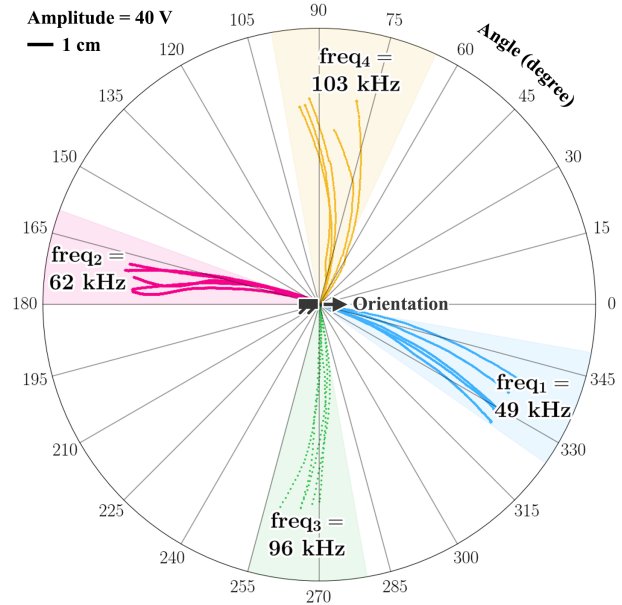

Fig. 8. Steering direction vs. actuation frequency plot. The initial orientation is 0°. Locomotion in all four principal directions were achieved at distinct frequencies. The lines/scattered dots show the trajectories.

Fig. 8 shows the frequency dependency of motion, with colored areas showing the selected principal directions, and lines/scattered dots showing the trajectories at the indicated frequencies [See Supplementary Video]. Starting at 49 kHz,

the robot moved forward with a slight right turn. At 62 kHz, the robot moved backward, as predicted by the theory in [21]. At 96 and 103 kHz, the robot turned right and left, respectively. The results verified the earlier discussion that steering can be achieved in bristle robots with the asymmetrical design.

The tethering wires were light, and made into a coiled shape that can better deform to accommodate locomotion in all directions. However, it was noticed that the motion was still affected to some extent by the wires' tension and mass loading. To avoid the wire tension in the future, we can integrate the power and electronics on top of the robot. Our robot is shown to have a payload over 13 g (65 times the polymer body weight), thus should be able to carry a commercially available coin battery together with a driver chip without failing.

B. Speed and Directionality

The robot's speed showed a frequency dependency as anticipated, matching our previous observation in [21]. The frequency spectrum of velocity is shown in Fig. 9. Each peak shows a different region of the locomotion. The different planes where each peak resides indicate the direction of motion. The height of the peak indicates the average speed in that particular direction. Forward, backward, left and right motions have velocities of 3.7 cm/s, 0.2 cm/s, 3.2 cm/s, and 6.3 cm/s, respectively. These velocities are equivalent to 3.1, 0.2, 2.6, and 5.2 body lengths per second, respectively.
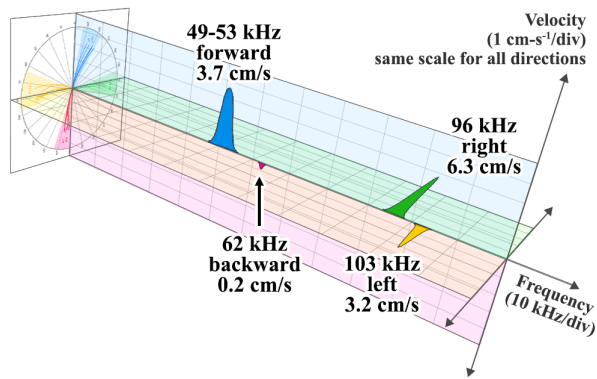

Fig. 9. Frequency spectrum of velocity. Different directions of motion showed different velocity.

Multiple trajectories for each direction were plotted in Fig. 8 to show the high repeatability of the steering. With a travel distance of 7.5 cm, the end points among multiple trials fell onto an angular region about 15° for all principal directions. This observation is different from our previously reported micro bristle robot results in [19], where a more random motion was observed. The difference is believed to be caused by not only the robot's larger size, but also the fact that it has more bristles so that the randomness of each individual bristle can be averaged out.

C. Minor Direction Steering by Superimposing Frequencies

After testing the bristle robot motion with individual actuation frequencies and achieving locomotion in all four principal directions, we tested the real-time superposition of two principal frequencies to show the capability of moving in minor directions and covering the full 360° 2D plane.
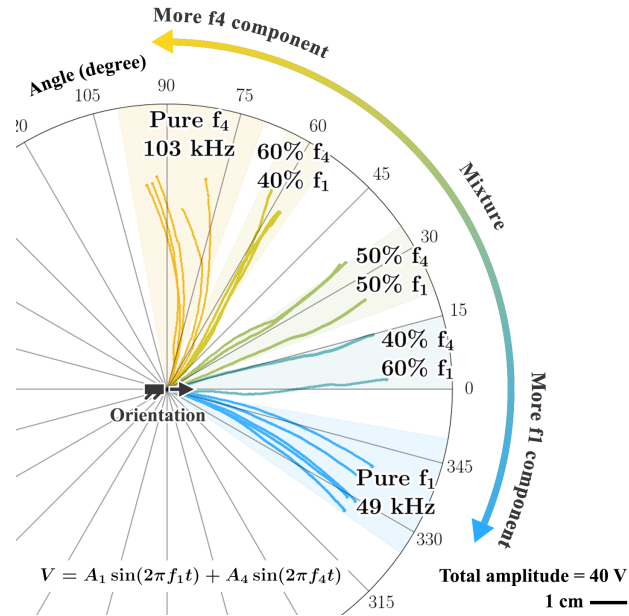

Fig. 10. Minor direction steering using superposition of frequencies. Two pure principal frequencies (49 kHz and 103 kHz) were superimposed with various amplitudes. The robot showed locomotion in minor directions determined by the mixing proportions, in between the two principal directions.

The result of mixing the forward frequency (f_1): 49 kHz and the left frequency (f_4): 103 kHz with different proportions is shown in Fig. 10. As shown, when the frequency components are mixed with equal amplitudes, the direction of motion is in the middle of the two principal directions. When one frequency component has a larger proportion, the robot moves towards that direction [See Supplementary Video]. This result shows that the robot can be actuated simultaneously at the superposition of multiple frequencies to achieve composite motions in between the principal directions, covering the full 360° 2D plane. This also suggests that the robot is able to transition seamlessly to move in a new direction at any time, simply by changing the mixing proportion.

VI. CONCLUSION AND FUTURE DIRECTIONS

We designed and fabricated a micro bristle robot with asymmetrical sides, where the left and right sets of bristles have different geometries and thus different resonant frequencies. This led to an asymmetrical bristle response, when the unibody robot was actuated at various frequencies. As a result, distinct frequency regions were determined and could be used to reliably steer the micro bristle robot in all four principal directions. It was also shown that by superimposing two of these principal frequencies with different amplitude

proportions, the robot can move in any directions in between, suggesting the ability to cover the full 360° 2D space.

The findings in this paper provide a new steering mechanism that simply depends on the bristle robot's geometry, making it suitable for miniaturized robotic systems. Such robots would be suitable for applications that require well-controlled and yet size/weight-limited locomotion, such as in vivo drug delivery, environmental conservation, and extraterrestrial explorations.

Future directions of the research include: 1) developing closed-loop systems with real-time feedback, 2) transitioning to untethered actuation (i.e. adding on-board power and electronics), 3) deploying swarm algorithms with multiple micro bristle robots.

ACKNOWLEDGMENT

REFERENCES

[1] G. Notomista, S. Mayya, A. Mazumdar, and S. Hutchinson, "A Study of a Class of Vibration-Driven Robots: Modeling, Analysis, Control and Design of the Brushbot," *arXiv.org*. [Online]. Available: http://arxiv.org/abs/1902.10830 [Accessed: 15-Sep-2019].

[2] S. Schwebke and C. Behn, "Worm-like robotic systems: Generation, analysis and shift of gaits using adaptive control," *Artificial Intelligence Research*, vol. 1, no. 2, p. 12, 2012.

[3] A. Gmiterko, M. Dovica, M. Kelemen, V. Fedak, and Z. Mlynkova, "In-pipe Bristled Micromachine," *Proceedings of 7th International Workshop on Advanced Motion Control*.

[4] S. Mayya, G. Notomista, D. Shell, S. Hutchinson, and M. Egerstedt, "Non-Uniform Robot Densities in Vibration Driven Swarms Using Phase Separation Theory," *arXiv.org*. [Online]. Available: http://arxiv.org/abs/1902.10662 [Accessed: 15-Sep-2019].

[5] K. Zimmermann, I. Zeidis, and C. Behn, Mechanics of terrestrial locomotion with a focus on non-pedal motion systems. *Dordrecht: Springer*, 2009.

[6] L. Sun, Y. Zhang, P. Sun, and Z. Gong, "Study on robots with PZT actuator for small pipe," *Proceedings of 2001 International Symposium on Micromechatronics and Human Science*.

[7] H. Park, B. Kim, J.O. Park, and S. J. Yoon, "A Crawling Based Locomotive Mechanism Using a Tiny Ultrasonic Linear Actuator (TULA)," *Proceedings of 39th Int. Symposium on Robotics*, pp. 85-90, 2008.

[8] M. Dovica, M. Gorzas, J. Kovac, S. Ondocko, "In-Pipe Passive Smart Bristled Micromachine," *SAMI 2004 - 2nd Slovakian – Hungarian Joint Symposium on Applied Machine Intelligence*.

[9] F. Becker, "An Approach to the Dynamics of Vibration-driven Robots with Bristles," *IFAC-PapersOnLine*, vol. 48, no. 1, pp. 842–843, 2015.

[10] F. Becker, S. Boerner, V. Lysenko, I. Zeidis, and K. Zimmermann, "On the Mechanics of Bristle-Bots - Modeling, Simulation and Experiments," *ISR/Robotik 2014; 41st International Symposium on Robotics*, 2014.

[11] K. Zimmermann, I. Zeidis, N. Bolotnik, and M. Pivovarov, "Dynamics of a two-module vibration-driven system moving along a rough horizontal plane," *Multibody System Dynamics*, vol. 22, no. 2, pp. 221–221, 2009.

[12] F. Chernousko, "The optimum rectilinear motion of a two-mass system," *Journal of Applied Mathematics and Mechanics*, vol. 66, no. 1, pp. 1–7, 2002.

[13] N. Bolotnik, S. Jatsun, A. Jatsun, and A. Cherepanov, "Automatically controlled vibration-driven robots," *2006 IEEE International Conference on Mechatronics*, 2006.

[14] Z. Wang and H. Gu, "A Bristle-Based Pipeline Robot for Ill-Constraint Pipes," *IEEE/ASME Transactions on Mechatronics*, vol. 13, no. 3, pp. 383–392, 2008.

[15] Z. Wang and E. Appleton, "The simulation and concept of a pipe crawling robot for earthquake rescue," *Proceedings of the International Conference on Control Applications*.

[16] H. Lu, J. Zhu, Z. Lin, and Y. Guo, "An inchworm mobile robot using electromagnetic linear actuator," *Mechatronics*, vol. 19, no. 7, pp. 1116–1125, 2009.

[17] L. Xu, H. Q. Chen, J. Zou, W. T. Dong, G. Y. Gu, L. M. Zhu, and X. Y. Zhu, "Bio-inspired annelid robot: a dielectric elastomer actuated soft robot," *Bioinspiration & Biomimetics*, vol. 12, no. 2, p. 025003, 2017.

[18] K. Ioi, "A mobile micro-robot using centrifugal forces," *1999 IEEE/ASME International Conference on Advanced Intelligent Mechatronics*, 1999.

[19] H. B. Fang and J. Xu, "Controlled motion of a two-module vibration-driven system induced by internal acceleration-controlled masses," *Archive of Applied Mechanics*, vol. 82, no. 4, pp. 461–477, Sep. 2011.

[20] D. Kim, Z. Hao, J. Ueda, and A. Ansari, "A 5g micro-bristle-bot fabricated by two-photon lithography," *Journal of Micromechanics and Microengineering*, vol. 29, no. 10, p. 105006, Jan. 2019.

[21] D. Kim, Z. Hao, A. R. Mohazab, and A. Ansari, "On the Forward and Backward Motion of Milli-Bristle-Bots," arXiv preprint arXiv:2002.10344, 2020.

[22] S. Chakraborty, Mechanics over micro and nano scales. New York: Springer, 2011.

[23] 3DSYSTEM, "ProJet 3500 SD & HD Professional 3D Printers," *3DSYSTEMS*. [Online]. Available: https://www.3dsystems.com/sites/default/files/projet_3500_plastic_01 15_usen_web.pdf [Accessed: 15-Sep-2019].

[24] 3DSYSTEM, "MultiJet Plastic Printers Functional Precision Plastic Parts with ProJet MJP 3D Printers," *3DSYSTEMS*. [Online]. Available: https://www.3dsystems.com/sites/default/files/2018-11/3d-systems-proJet-mjp-3600-plastic-tech-specs-usen-2018-11-08-web.pdf [Accessed: 15-Sep-2019].

[25] APC International, "Physical and Piezoelectric Properties of APC Materials," *APC International*. [Online]. Available: https://www.americanpiezo.com/apc-materials/physical-piezoelectric-properties.html. [Accessed: 15-Sep-2019].

[26] M. Rubenstein, C. Ahler, and R. Nagpal, "Kilobot: A low cost scalable robot system for collective behaviors," *2012 IEEE International Conference on Robotics and Automation*, 2012.